iScience

CellPress
OPEN ACCESS

Article

Circulation immune cell landscape in canonical pathogenesis of colorectal adenocarcinoma by CyTOF analysis

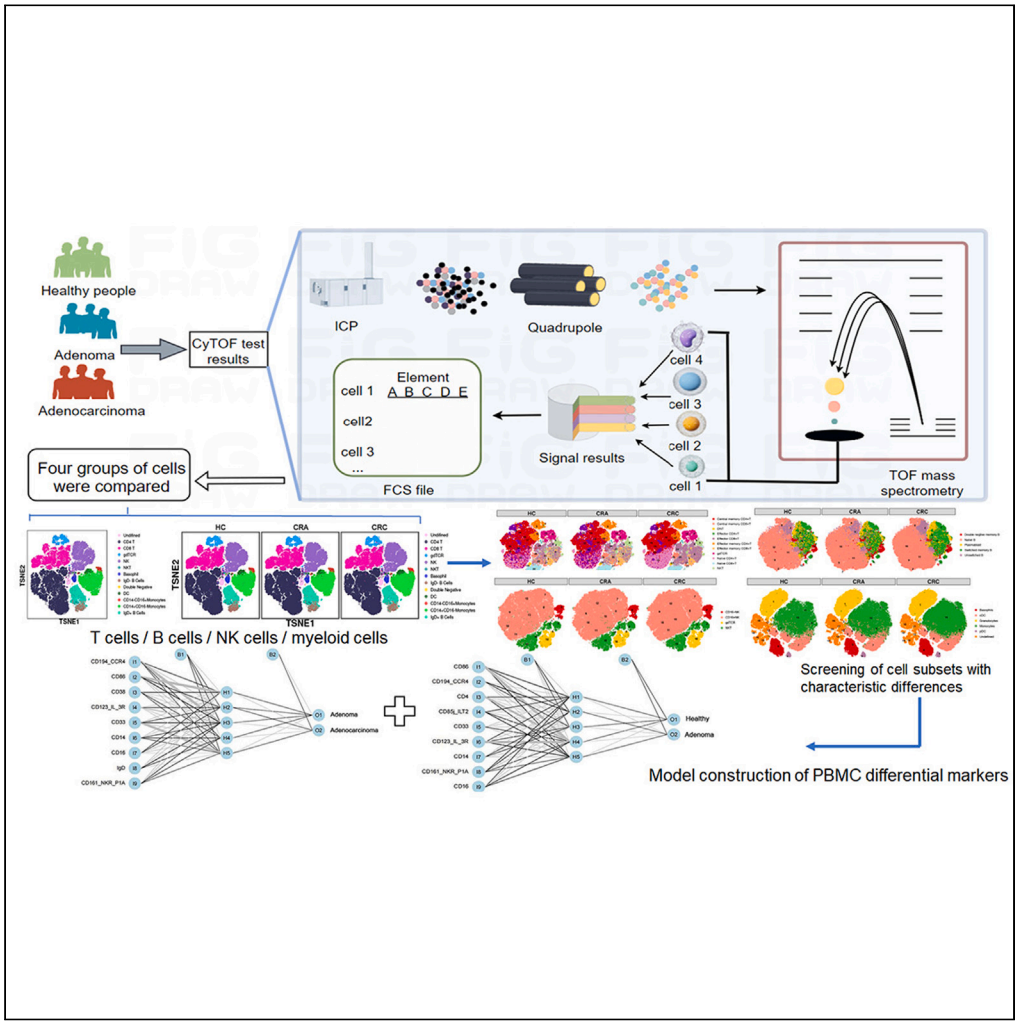

Xiang-Xing Kong, Jia-Sheng Xu, Ye-Ting Hu, ..., Xu-Ran Hao, Jun Li, Ke-Feng Ding

2307016@zju.edu.cn (J.L.)
dingkefeng@zju.edu.cn (K.-F.D.)

Highlights

Drawing landscape of peripheral blood immune cell subsets for CRC carcinogenesis

Monocytes play the key role in CRC carcinogenesis

Provide future biomarkers for immunotherapy

Kong et al., iScience 27, 109229
March 15, 2024
https://doi.org/10.1016/j.isci.2024.109229

iScience

CellPress
OPEN ACCESS

Article

Circulation immune cell landscape in canonical pathogenesis of colorectal adenocarcinoma by CyTOF analysis

Xiang-Xing Kong,[1,6] Jia-Sheng Xu,[1,6] Ye-Ting Hu,[1,6] Yu-Rong Jiao,[1,6] Sheng Chen,[1] Cheng-Xuan Yu,[1] Si-Qi Dai,[1] Zong-Bao Gao,[5] Xu-Ran Hao,[5] Jun Li,[1,*] and Ke-Feng Ding[1,2,3,4,7,*]

SUMMARY

Current studies on the immune microenvironment of colorectal cancer (CRC) were mostly limited to the tissue level, lacking relevant studies in the peripheral blood, and failed to describe its alterations in the whole process of adenocarcinoma formation, especially of adenoma carcinogenesis. Here, we constructed a large-scale population cohort and used the CyTOF to explore the changes of various immune cell subsets in peripheral blood of CRC. We found monocytes and basophils cells were significantly higher in adenocarcinoma patients. Compared with early-stage CRC, effector CD4$^+$T cells and naive B cells were higher in patients with lymph node metastasis, whereas the basophils were lower. We also performed random forest algorithm and found monocytes play the key role in carcinogenesis. Our study draws a peripheral blood immune cell landscape of the occurrence and development of CRC at the single-cell level and provides a reference for other researchers.

INTRODUCTION

Colorectal cancer (CRC) is the third most frequently diagnosed cancer and the second leading cause of mortality worldwide, and the canonical adenoma–carcinoma sequence has been widely recognized for the development of sporadic CRC.[1–4] Current studies have identified genetic alterations,[5] microbial biomarkers, and liquid biopsies[6,7] as potential diagnostic and treatment tools for CRC. Jun Yu et al. performed metagenome profiling on feces to discover and validate microbial biomarkers[8,9]; they later demonstrated that intra-neoplasia microbiota is correlated with CRC proliferation.[10,11] Therefore, we believe the internal environment adjusts significantly during the development of CRC, which can be detected and may contribute to the diagnosis and treatment.

Tumor-infiltrated immune cells regulate cancer progression and are considered attractive immunotherapy targets.[12–14] Jérôme Galon et al. characterized the type, density, and location of immune cells within CRC, which is a significant finding. They also validated its predictive value and established a robust recurrence risk assessment model named Immunoscore for colon cancer.[15–18] Zemin Zhang's group quantitatively analyzed the dynamic relationships among 20 identified T cell subsets by single-cell sequencing.[19] They identified specific macrophage and dendritic cells (DC) that convey differential sensitivity to CSF1R blockade and defined concerted immune responses involving DC cells and T cells upon anti-CD40 treatment.[20] The analyses of CD45$^+$ cells simultaneously from matched tissues of treatment-naive hepatocellular carcinoma, CRC, and CRC liver metastasis delineated a comprehensive landscape of immune compartments among these different tissues.[21] In light of these results, we believe the dynamics in immune cells play an essential role in the occurrence and progression of CRC. However, most studies focused on depicting the differences in tissue level, whereas alterations of immune cells in peripheral blood mononuclear cells (PBMCs) were overlooked.

Cytometry by time-of-flight mass spectrometry (CyTOF) is a new high-dimensional multi-parameter analysis technology with multiple measurement parameters and high single-cell recognition accuracy.[22,23] It can detect more than 40 markers simultaneously at single-cell level and conduct more in-depth research on cell phenotypes, signal pathways, and functions.[24] Steele et al. performed CyTOF on pancreatic ductal adenocarcinoma (PDAC), normal/adjacent uninvolved tissue samples, and matched PBMCs. They observed a higher frequency of TIGIT on CD8$^+$ T cells in the tumor. Moreover, the expression of TIGIT in CD8$^+$ T cells was positively correlated in tumor and PBMCs.[25] Another study determined the alterations of peripheral immune cell subsets caused by hepatocellular carcinoma (HCC) or PDAC through CyTOF analysis for

[1]Department of Colorectal Surgery and Oncology (Key Laboratory of Cancer Prevention and Intervention, China National Ministry of Education), The Second Affiliated Hospital, Zhejiang University School of Medicine, Hangzhou, Zhejiang, China
[2]Center for Medical Research and Innovation in Digestive System Tumors, Ministry of Education, Hangzhou, China
[3]Zhejiang Provincial Clinical Research Center for CANCER, Hangzhou, China
[4]Cancer Center of Zhejiang University, Hangzhou, China
[5]Zhejiang Puluoting Health Tech CO. LTD, Hangzhou, China
[6]These authors contributed equally
[7]Lead contact
*Correspondence: 2307016@zju.edu.cn (J.L.), dingkefeng@zju.edu.cn (K.-F.D.)
https://doi.org/10.1016/j.isci.2024.109229

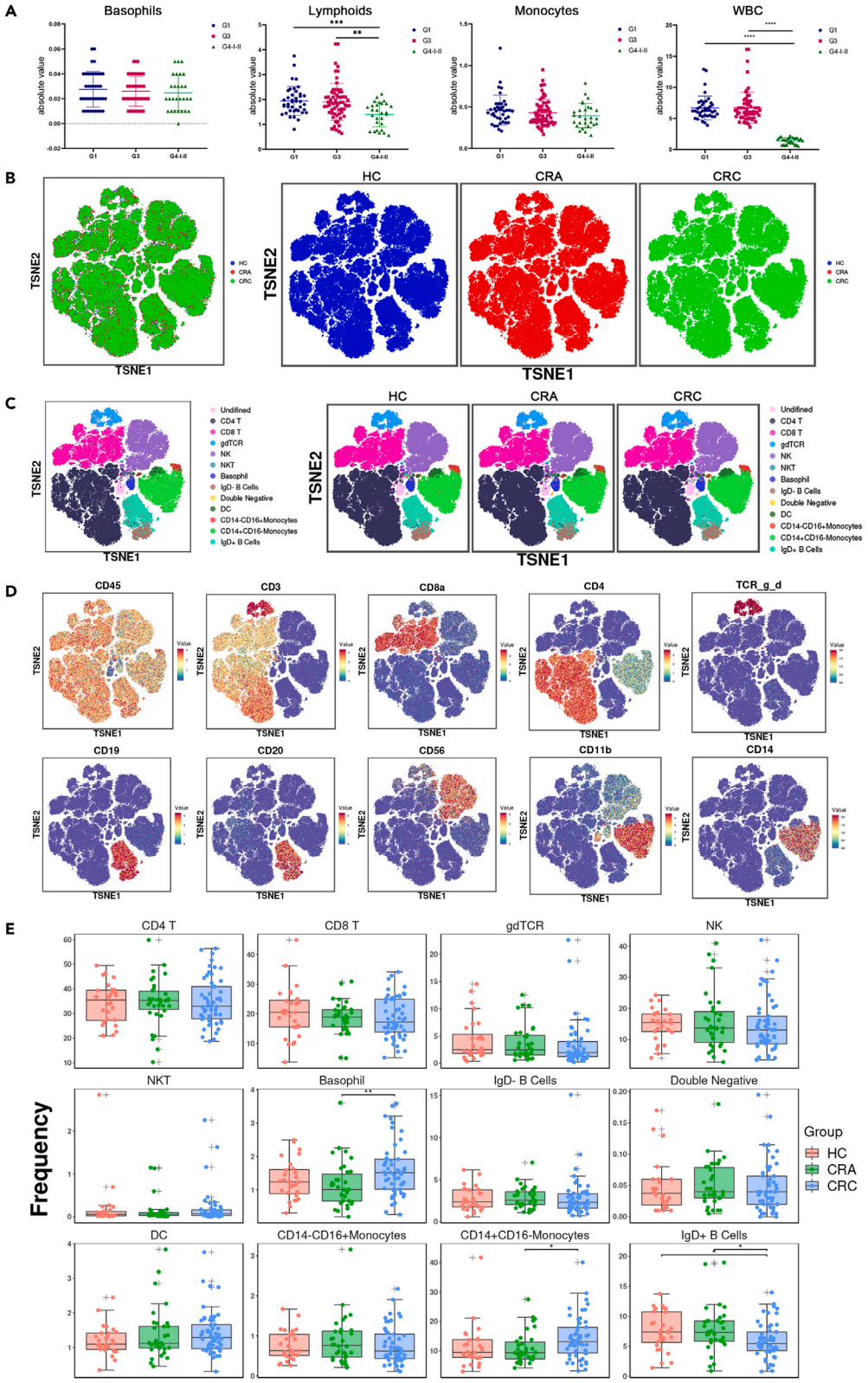
A
Basophils
Lymphoids
Monocytes
WBC
absolute value
G1
G3
G4-I-II
B
HC
CRA
CRC
TSNE1
TSNE2
C
Undifined
CD4 T
CD8 T
gdTCR
NK
NKT
Basophil
IgD- B Cells
Double Negative
DC
CD14-CD16+Monocytes
CD14+CD16-Monocytes
IgD+ B Cells
D
CD45
CD3
CD8a
CD4
TCR_g_d
CD19
CD20
CD56
CD11b
CD14
Value
E
CD4 T
CD8 T
gdTCR
NK
NKT
Basophil
IgD- B Cells
Double Negative
DC
CD14-CD16+Monocytes
CD14+CD16-Monocytes
IgD+ B Cells
Frequency
Group
HC
CRA
CRC

Figure 1. Overall differences of each immune cell group in PBMC in healthy human, adenoma, and adenocarcinoma patients

(A) Comparison of blood routine results in normal people, adenoma patients, and stage I and II adenocarcinoma patients.

(B) Display of the overall expression of $CD45^+$ cells in the three groups of patients.

(C) The overall immune cell expression of the three groups of patients and the t-SNE results of the comparative analysis between the groups.

(D) The expression of the main cell classification markers in all the samples included in the group: CD45: white blood cell marker; CD3: T cell marker; CD19: B cell marker; CD56: NK cells.

(E) The overall difference of immune cells among the three groups. Asterisk was used to indicate the significance of the expression difference between the groups. *$p < 0.05$, **$p < 0.01$, ***$p < 0.001$.

peripheral blood. They also established models based on selected cell markers and subsets obtained from CyTOF in detecting patients with malignancies.[26]

In CRC, there was still a lack of large-scale studies on the alterations in peripheral blood immune cells in the whole process of adenocarcinoma formation. Herein, we performed CyTOF analysis of PBMC samples from 102 CRCs, 47 adenomas, and 42 healthy volunteers. We mapped the dynamic changes of peripheral blood immune cell profiles during the development and progression of CRC: central memory $CD4^+$ T cells and switched memory B cells increased in adenocarcinoma, whereas naive double-negative T cell (DNT) level decreased in adenoma and adenocarcinoma. The expression of $CD16^-$ natural killer (NK) cell subsets was significantly higher in adenocarcinoma compared with normal and adenomas; monocytes and basophils were significantly higher in adenocarcinoma patients compared with adenoma patients.

Our research reported the changes in subpopulation and number of immune cells during the course of the occurrence and development of colorectal adenocarcinoma. This research hinted at the potential biomarkers for future immunotherapy and provided a reference for the analysis of immune profiles of other tumor types.

RESULTS

Characteristics of the participants

The present study finally enrolled 191 participants from our medical center. Among them, 42 were healthy volunteers (Group HC). Forty-seven were diagnosed with colorectal adenoma (Group CRA), 26 with low-grade adenoma, and 21 with high-grade adenoma. Group CRC included 102 patients diagnosed with colorectal adenocarcinoma, with 15 stage I, 45 stage II, and 42 stage III according to the 8^{th} AJCC TNM staging system.

Peripheral blood samples were collected from all enrolled participants. We firstly performed routine blood test and compared white blood cells (WBCs) and their components within HC, CRA, and early-stage CRC to explore the alterations during carcinogenesis. Compared with HC and CRA, stage I and II CRC had lower total white blood cells (6.685 vs. 1.898, $p < 0.05$) and lymphocytes (1.944 vs. 1.394, $p < 0.05$). Basophils and monocytes were not significantly different among the three groups ($p > 0.05$) (Figure 1A). Therefore, we believe the differences in leukocyte subsets are worth further exploring.

Twelve defined peripheral immune cell subgroups were annotated by CyTOF

The total leukocytes were displayed by annotating $CD45^+$ cells, and its expression showed no significant difference within the three groups (Figure 1B). We then analyzed the expression of 40 markers and clustered all cells into 12 defined immune cells after annotation, including CD4 T cells, CD8 T cells, double-negative T cells, nature killer T cells (NKT), $CD14^-CD16^+$ monocytes, $CD14^+CD16^-$monocytes, $gdTCR^+$ T cells, IgD^- B cells, IgD^+ B cells, NK cells, DC, and basophils (Figures S1A and S1B).

In the three groups of patients, we counted the percentage of T cells, B cells, NK cells, and myeloid cell subsets and found that the proportion of $CD14^+$ monocytes in PBMC was increased in the adenocarcinoma group, as compared with the other two groups (Figures S2A–S2C). Moreover, the proportion of further divided subsets in T cells, B cells, NK cells, and myeloid cells in Group HC, CRA, and CRC was statisted respectively, and the results were showed in Figures S2D–S2O. We then compared the annotated immune cell subgroups via ViSNE, and the marker gene of each main subgroup was also displayed (Figures 1C and 1D). The frequency of $CD14^+CD16^-$monocytes and basophils in CRC was higher than that in CRA, whereas the frequency of IgD^- B cells was significantly lower (Figure 1E). Because few significant differences were detected among the three groups in 12 major peripheral blood subgroups, we would further explore the differences in T cells, B cells, NK cells, and myeloid cells among the three groups.

CyTOF results of T cells

T cells were sorted through $CD45^+CD3^+CD19^-$ and then classified into 27 subclusters via t-SNE (Figures 2A, 2B, and S3A). A total of 26 markers were obtained through clustering. Compared with CRA, CD45 and CCR4 were increased in CRC patients. PD1 was decreased in CRA when compared with HC (Figure S3B). The expression of the 26 markers in 27 clusters among three groups were displayed, respectively (Figures S3C–S3F). Later, a total of 12 defined T cell subgroups were obtained, and the difference of the corresponding clusters of T cells within the three groups was performed (Figure 2C). Naive $CD8^+$ T cells and DNT cells were lower in CRA and CRC compared with HC. Treg cells and central memory $CD8^+$ T cells in CRA were higher than HC (Figure 2D).

CyTOF test results of B cells

T-SNE dimensionality reduction analysis was performed on the B cells, and they were divided into 13 clusters (Figures 3A, 3B, and S4A). There were 17 types of markers in the obtained B cells. CD45 and CD24 were more expressed in CRC than CRA; HLA^-DR is reduced in CRA and CRC

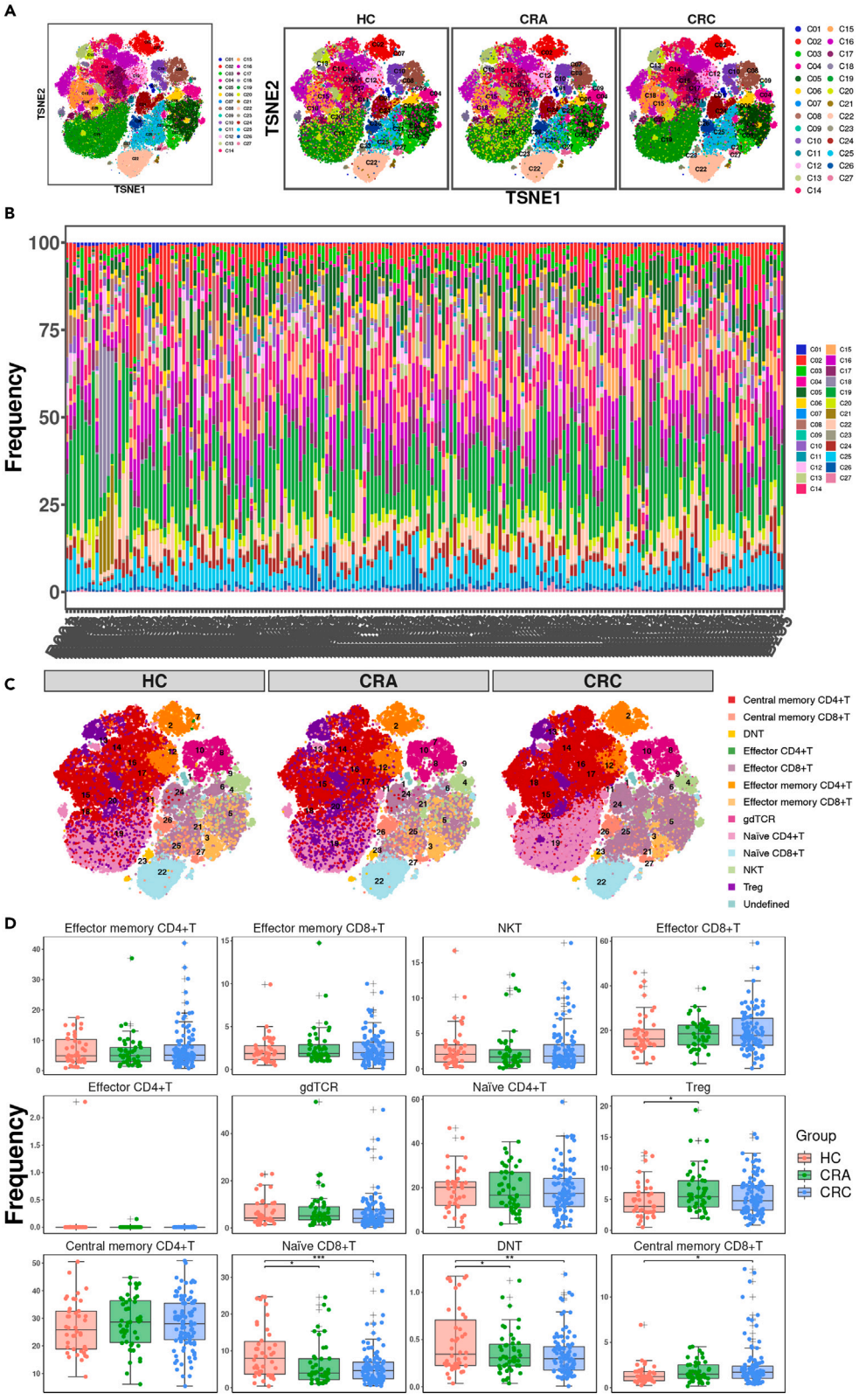
A
HC
CRA
CRC
TSNE1
TSNE2
B
Frequency
100
75
50
25
0
C
HC
CRA
CRC
Central memory CD4+T
Central memory CD8+T
DNT
Effector CD4+T
Effector CD8+T
Effector memory CD4+T
Effector memory CD8+T
gdTCR
Naïve CD4+T
Naïve CD8+T
NKT
Treg
Undefined
D
Effector memory CD4+T
Effector memory CD8+T
NKT
Effector CD8+T
Effector CD4+T
gdTCR
Naïve CD4+T
Treg
Central memory CD4+T
Naïve CD8+T
DNT
Central memory CD8+T
Frequency
Group
HC
CRA
CRC

Figure 2. Differences in the expression of T cell subsets in peripheral blood of healthy people, adenomas, and adenocarcinoma patients

(A) The t-SNE results of the T cell classification of the three groups of patients are displayed.

(B) The heatmap display of the expression of T cell clusters in the three groups of patients.

(C) The t-SNE results of classification of T cells subgroups annotated by 27 clusters.

(D) Comparison results of the expression differences of 12 types of T cell subsets among the three groups. Asterisk was used to indicate the significance of the expression difference between the groups.

*$p < 0.05$, **$p < 0.01$, ***$p < 0.001$.

compared with HC (Figure S4B). The expression of 17 markers in 13 clusters of B cells were also shown (Figures S4C–S4F). We then annotated the 13 clusters and obtained 5 B cell subgroups (Figures S4G and S4C). The differences in B cell subgroups among the three groups were displayed while the results showed no significant difference (Figure 3D).

CyTOF test results of NK cells

NK cell marker genes were clustered, and a total of 16 clusters were obtained (Figure 4A). The proportion of the 16 NK cell clusters in the three groups was compared, and the heatmap was drawn (Figure 4B). Compared with HC and CRA, cluster 01 was significantly decreased in CRC, and cluster 03 was significantly increased in CRC. Compared with HC, cluster 02 was increased in CRC, cluster 03 was significantly increased in CRA, cluster 07 was significantly decreased in CRC, and cluster 10 was significantly increased in CRA (Figure S5A). The differential expression of 16 NK cell clusters in the three groups was shown in Figure S5B. The obtained NK cells contained a total of 18 markers. In detail, CD56 in CRC was increased than CRA; CD11c in CRA, CD16 in CRC, and CD94 in both CRA and CRC were decreased than HC (Figure S5B). The expression of the 18 markers in 16 clusters among three groups were displayed respectively (Figures S5C–S5F). After annotation, four defined subgroups related to NK cells were yielded (Figure 4C). Compared with HC, $CD11b^{+}CD16^{-}$ NK cells were increased in CRC, and $CD11b^{-}CD16^{-}$ NK cells gradually increased in CRA and CRC. However, $CD16^{+}$ NK cells decreased in CRC, and $CD57^{+}CD16^{+}$ NK cells decreased in CRA (Figure 4D).

CyTOF test results of myeloid cells

After clustering the myeloid cell marker genes from three groups, we obtained 17 clusters (Figure 5A). Compared with HC and CRA, cluster 10 significantly increased in CRC. Compared with HC, cluster 02, cluster 03, cluster 11, cluster 14, and cluster 15 were lower in CRC. Cluster 05 was increased in CRC compared with CRA (Figure S6A). The obtained myeloid cells contained 19 markers (Figure S6B). Comparative analysis of the expression of each marker in three groups showed that expression of CD86, CD33, CD38, and CCR4 were higher in CRC than in CRA, and CD16 was reduced in CRC. Compared with HC, the expression of CD14, CD86, CD33, CD38, CCR4, and CD4 climbed in CRC patients, and the expression of CD66b and CD16 dropped (Figure S6B). We compared the proportion of 17 clusters in the total myeloid cell population of patients in the three groups and drew the heatmap (Figure 5B). Expression of 19 markers of myeloid cells in 17 clusters in the HC, CRA, and CRC were displayed respectively (Figures S6C–S6F). We annotated 17 clusters and obtained 6 subgroups related to myeloid cells (Figure 5C). Compared with patients in CRA, basophils climbed in CRC patients; monocytes are more expressed in CRC patients than in HC and CRA (Figure 5D).

Circulation immune cell alterations in adenoma cancerization and lymph node metastasis

Adenoma carcinogenesis is the key process during adenocarcinoma formation. Identifying major cell subpopulation differences between adenoma and early-stage adenocarcinoma may help explore mechanisms associated with carcinogenesis. We firstly analyze the differences in T cell clusters between patients with adenoma and stage I adenocarcinoma. Twenty-seven T cell clusters were annotated into 13 T cell types (Figure 6A). However, comparative analysis did not yield significant differences in T cell subsets between the two groups (Figure 6B). We also annotated five B cell subsets and four NK cell subsets between both groups but detected no differences (Figures 6C–6F). Myeloid cell clusters were annotated into six myeloid cell subsets (Figure 6G). Basophils and monocytes were increased in stage I CRC compared with CRA, which suggests its role in CRC cancerization (Figure 6H).

Lymph node metastasis is a crucial risk factor for CRC prognosis and is definitive for treatment strategies. It has clinical urgency to explore the changes in immune cell subsets related to lymph node involvement. Therefore, we annotated T cell subsets of lymph nodes metastatic (stage III) CRC and non-metastatic (stage I and II) CRC. Twenty-seven clusters were labeled as 11 T cell subsets (Figure 7A). Effector $CD4^{+}$ T cells were higher in CRC patients with lymph node metastasis (Figure 7B). Sixteen B cell clusters were obtained, and five B cell subsets were finally annotated (Figure 7C). Naive B cell was significantly increased, and unswitched B-cell and plasma blast cell were both significantly lower in lymph node metastasis CRC (Figure 7D). NK cells were annotated into four NK cell subsets but there was no significant difference between groups (Figures 7E and 7F). Six myeloid cell subsets were annotated, and we found basophils were lower in lymph node metastasis CRC (Figures 7G and 7H).

Monocytes altered most significantly during colorectal carcinogenesis

We summarized the significant alterations in the proportion of each subpopulation in peripheral blood in each stage of colorectal carcinogenesis (Table 1). It suggests that immune cell subpopulations may be an important reference indicator for early detection of intestinal adenocarcinoma. However, it is still unclear which subsets are more important. Therefore, we performed a random forest algorithm to analyze

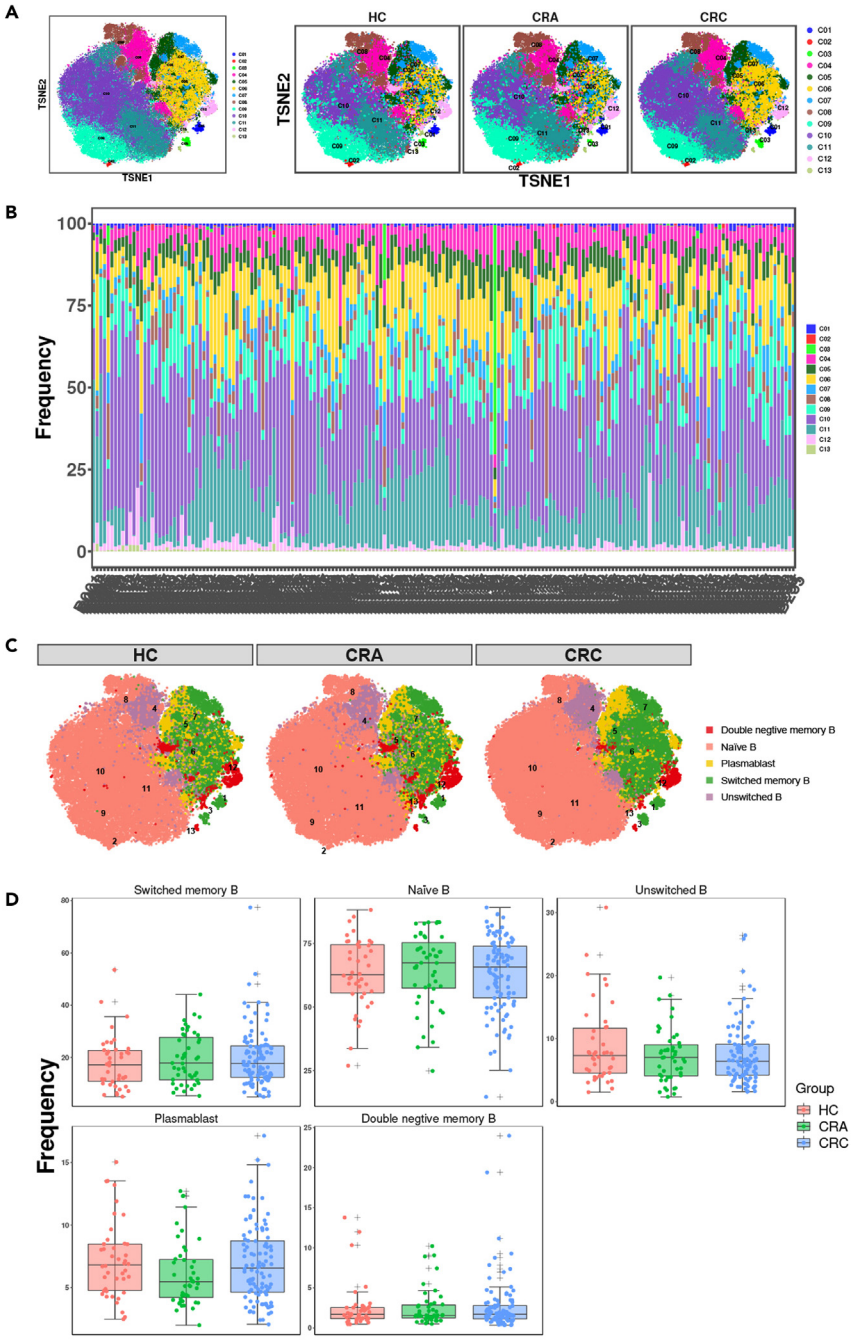

Figure 3. Differences in the expression of B cell subsets in peripheral blood of healthy people, adenomas, and adenocarcinoma patients

(A) The t-SNE results of the B cell classification of the three groups of patients are displayed.

(B) The heatmap display of the expression of B cell clusters in the three groups of patients.

(C) The t-SNE results of classification of B cells subgroups annotated by 13 clusters.

(D) Comparison results of the expression differences of five types of B cell subsets among the three groups.

*p < 0.05, **p < 0.01, ***p < 0.001.

immune cell surface markers and screened nine characteristic markers of adenomatosis (HC vs. CRA). They were ranked in descending order based on Mean Decrease Gini (MDG) as CD86, CD194_CCR4, CD161_NKR_P1A, CD4, CD85_ILT2, CD16, CD33, CD123_IL_3R, and CD14 (Figure S7A). We further mapped the nodes of action and neuro-modulatory networks of nine key genes to demonstrate how these markers respond to CRC features when paired in combination (Figure S7B).

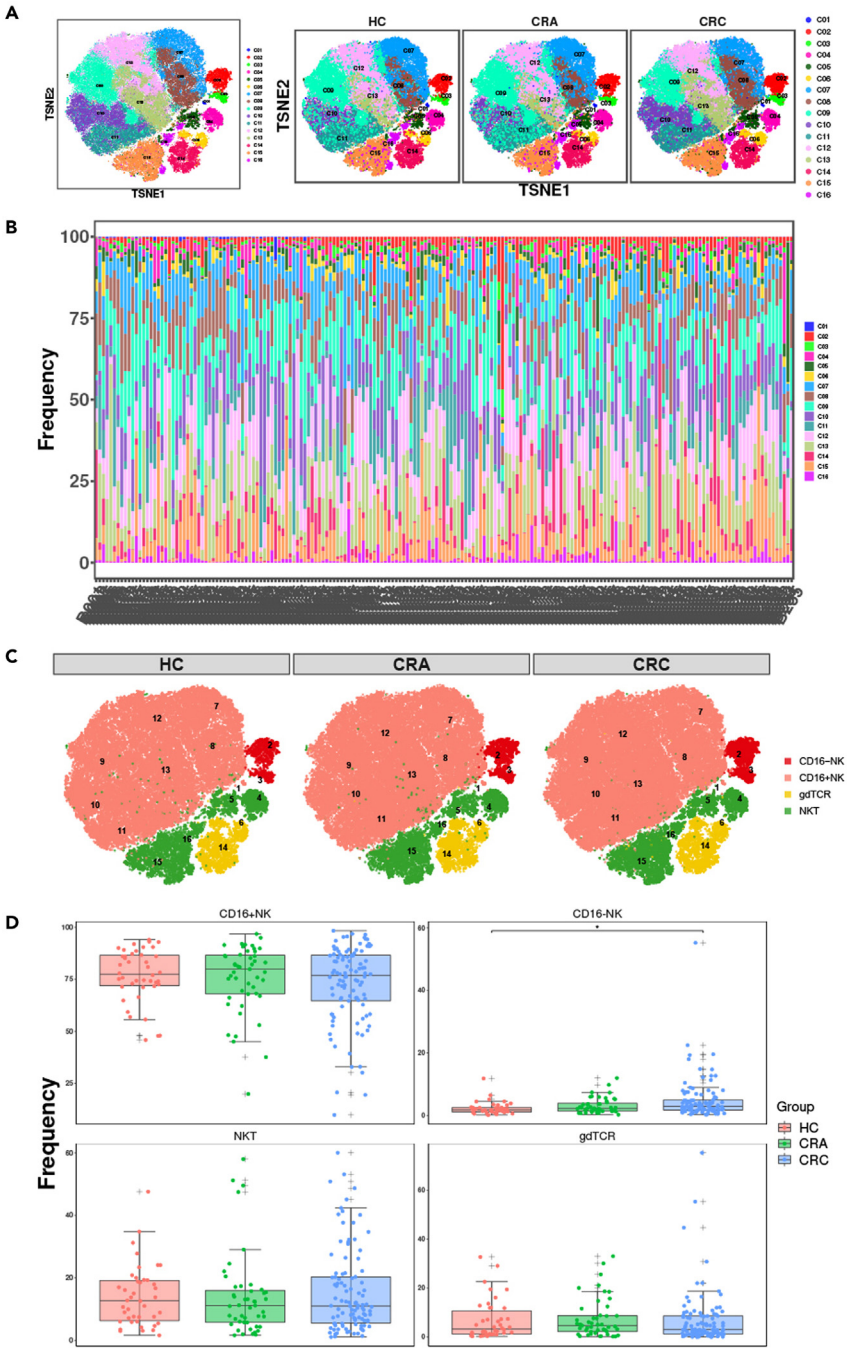

Figure 4. Differences in the expression of NK cell subsets in peripheral blood of healthy people, adenomas, and adenocarcinoma patients

(A) The t-SNE results of the NK cell classification of the three groups of patients are displayed.

(B) The heatmap display of the expression of NK cell clusters in the three groups of patients.

(C) The t-SNE results of classification of NK cells subgroups annotated by 16 clusters.

(D) Comparison results of the expression differences of four types of NK cell subsets among the three groups. Asterisk was used to indicate the significance of the expression difference between the groups.

*p < 0.05, **p < 0.01, ***p < 0.001.

We then followed the same process to analyze differentially expressed markers during adenocarcinoma carcinogenesis. Similarly, we screened nine markers that may affect adenocarcinoma carcinogenesis (CRA vs. CRC) and used neural network plots to demonstrate the associations that exist between these markers (Figures S7C and S7D). Comparing these nine markers (CRA vs. CRC) with the nine

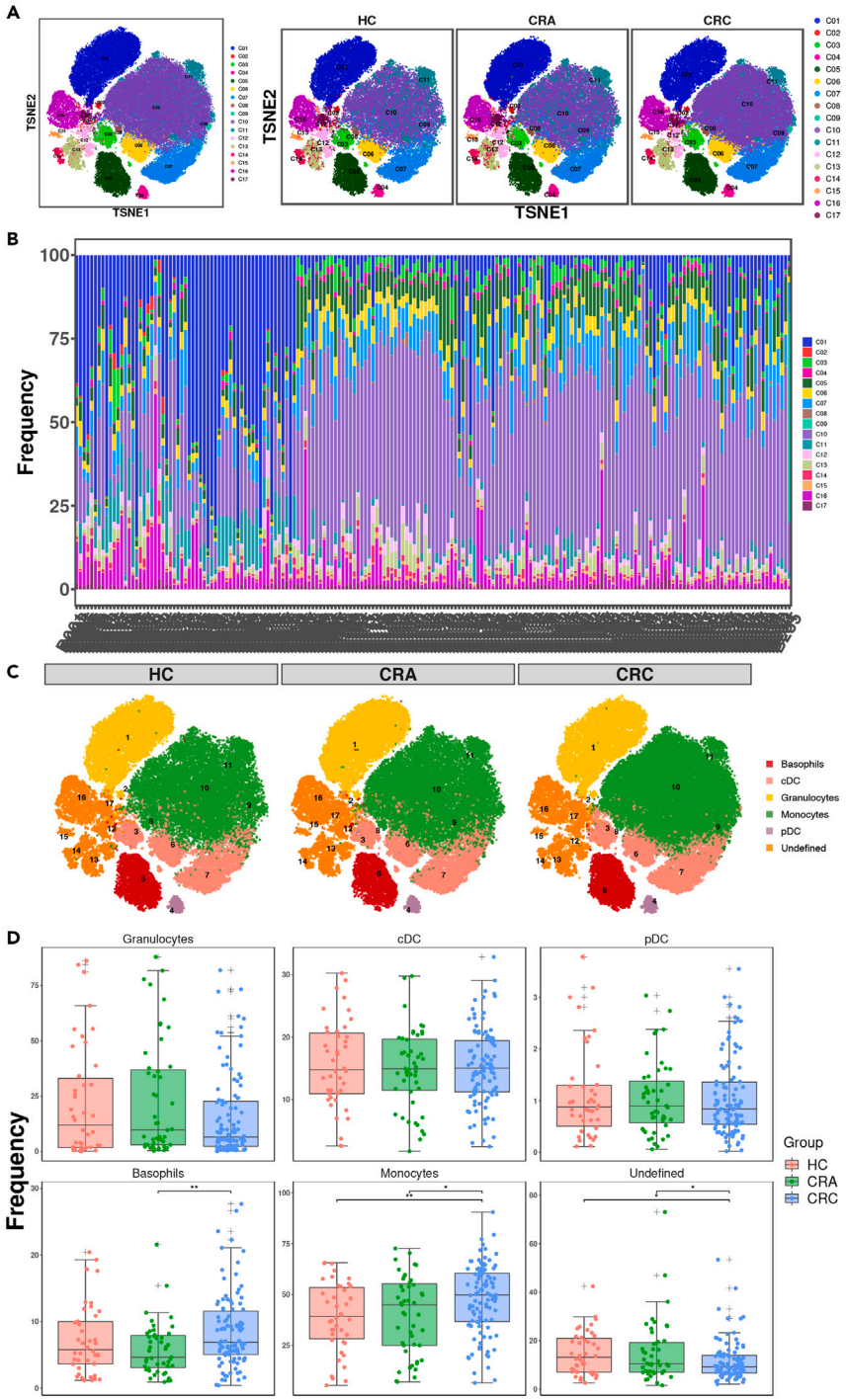

Figure 5. Differences in the expression of myeloid cell subsets in peripheral blood of healthy people, adenomas, and adenocarcinoma patients

(A) The t-SNE results of the myeloid cell classification of the three groups of patients are displayed.

(B) The heatmap display of the expression of myeloid cell clusters in the three groups of patients.

(C) The t-SNE results of classification of myeloid cells subgroups annotated by 17 clusters.

(D) Comparison results of the expression differences of six types of myeloid cell subsets among the three groups. Asterisk was used to indicate the significance of the expression difference between the groups.

*p < 0.05, **p < 0.01, ***p < 0.001.

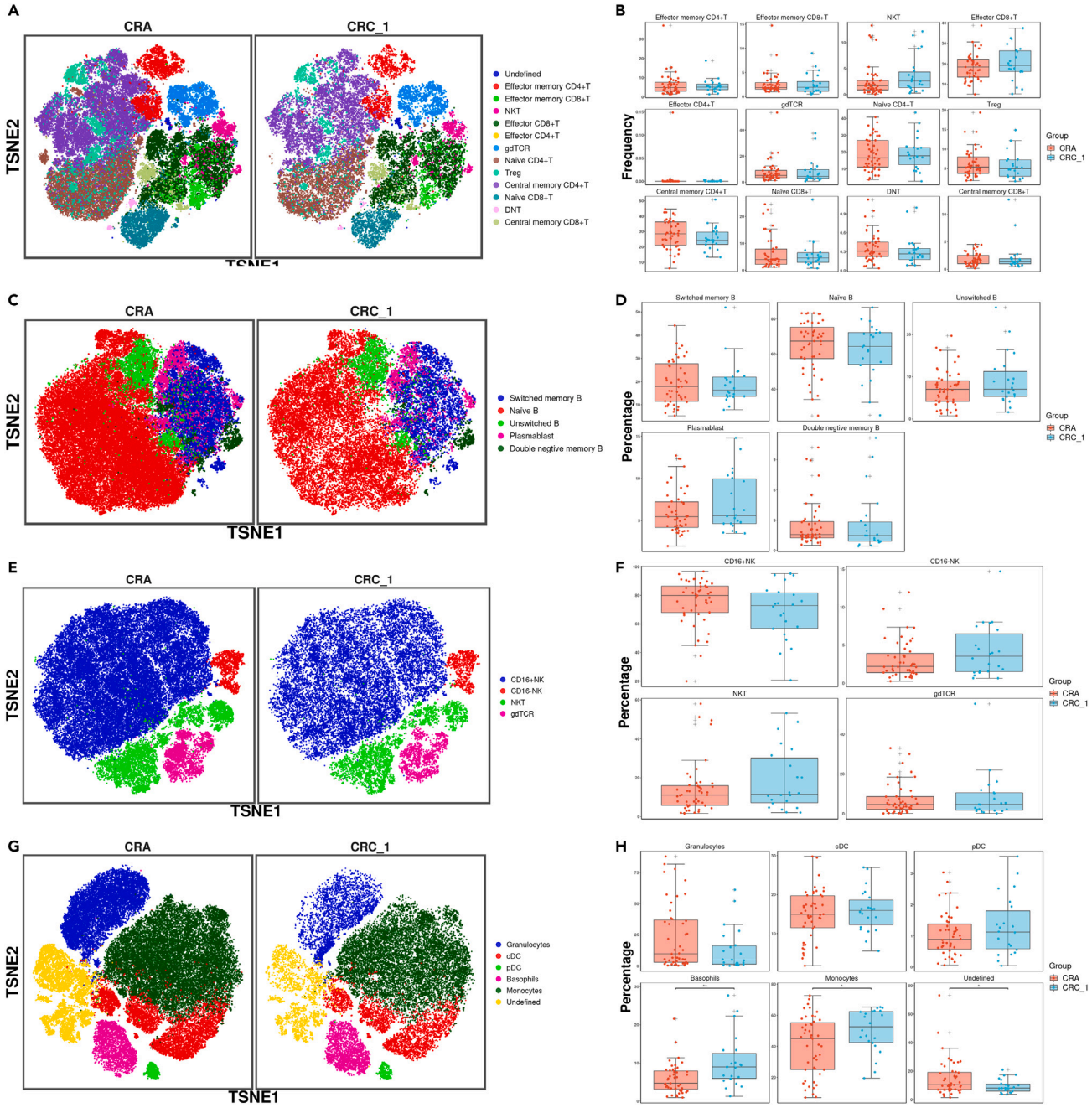

Figure 6. The proportion difference of immune cell subsets in PBMC of patients with adenoma and stage I colorectal cancer

(A) The t-SNE results of comparison of cell subpopulations of T cell in patients with adenoma and stage I adenocarcinoma.

(B) A histogram showing the comparison of 12 types of T cell subpopulations in adenoma and stage I adenocarcinoma.

(C) The t-SNE results of comparison of cell subpopulations of B cell in patients with adenoma and stage I adenocarcinoma.

(D) A histogram showing the comparison of five types of B cell subgroups in adenoma and stage I adenocarcinoma.

(E) The t-SNE results of comparison of cell subpopulations of NK cell in patients with adenoma and stage I adenocarcinoma.

(F) A histogram showing the comparison results of four types of NK cell subgroups in patients with adenoma and stage I adenocarcinoma.

(G) The t-SNE results of comparison of cell subpopulations of myeloid cell in patients with adenoma and stage I adenocarcinoma.

(H) A histogram showing the comparison of six types of myeloid cell subgroups in adenoma and stage I adenocarcinoma. Asterisk was used to indicate the significance of the expression difference between the groups.

*$p < 0.05$, **$p < 0.01$, ***$p < 0.001$.

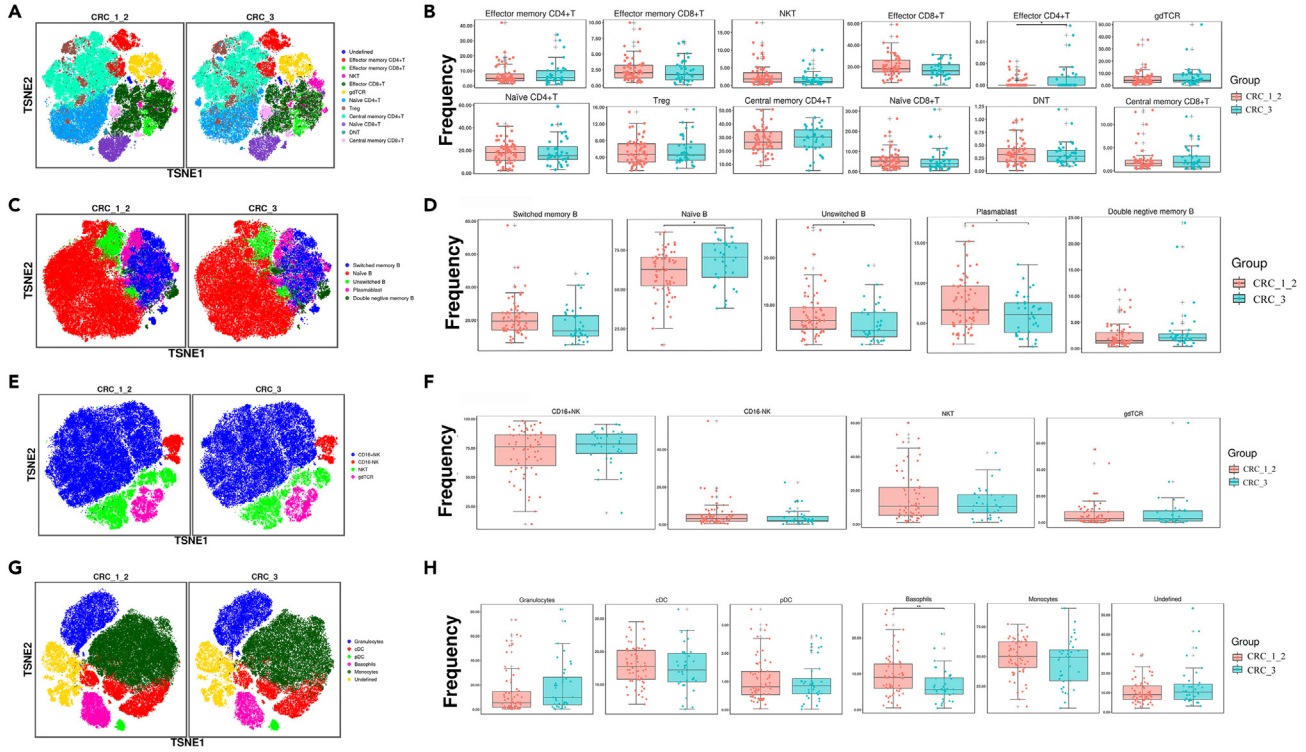

Figure 7. The proportion difference of immune cell subsets in PBMC of patients with lymph node metastasis and non-metastasis colorectal cancer

(A) The t-SNE results of comparison of cell subpopulations of T cell in patients with stage II and stage III adenocarcinoma.

(B) The histogram of the comparison of 12 types of T cell subgroups in colorectal cancer with or without lymph node metastasis.

(C) The t-SNE results of comparison of cell subpopulations of B cell in patients with stage II and stage III adenocarcinoma.

(D) The histogram of the comparison of five types of B cell subgroups in colorectal cancer with or without lymph node metastasis.

(E) The t-SNE results of comparison of cell subpopulations of NK cell in patients with stage II and stage III adenocarcinoma.

(F) The histogram of the comparison of four NK cell subgroups in colorectal cancer with or without lymph node metastasis.

(G) The t-SNE results of comparison of cell subpopulations of myeloid cell in patients with stage II and stage III adenocarcinoma.

(H) The histogram of the comparison of six types of myeloid cell subgroups in colorectal cancer with or without lymph node metastasis. Asterisk was used to indicate the significance of the expression difference between the groups.

*$p < 0.05$, **$p < 0.01$, ***$p < 0.001$.

markers detected earlier (HC vs. CRA), we revealed seven of them overlap. These seven markers may be focal markers associated with colorectal carcinogenesis. CD86 and CD14 are monocyte-related markers, except for CD194, CD161, and CD33, which are widely expressed in immune cells. This suggests that monocytes may play a key role in colorectal carcinogenesis. We then used flow cytometry to analyze $CD14^+$ monocyte and $CD14^+CD16^+$ monocyte in three groups. The expression of $CD14^+$ monocyte gradually increased in all three groups, whereas the expression of $CD14^+CD16^+$ monocyte gradually decreased, especially shown in T group, which dropped to 0.12% (Figures S7E–S7H).

DISCUSSION

In recent years, the recognition of immunity has grown wider in the treatment for CRC.[27] Numerous studies have demonstrated the immune microenvironment is closely related to the occurrence and progression of CRC.[28–32] However, these studies mainly investigated the infiltration of immune cells in cancer and matched normal tissues. Considering that clinical tumor screening for patients mainly relies on liquid biopsy, the characteristics of multi-stage in PBMC need to be studied. Ting Zhang et al.[33] performed CyTOF detection on PBMC of HC and CRC patients; they demonstrated the systemic and comprehensive expression profile of EpCAM, PD-1, and PD-L1 by T cells and their various subsets. Limited by the number of markers and the sample size, their study did not include adenoma patients. Their research mainly focused on T cells and lacked in-depth exploration of other PBMCs. Krijgsman D et al.[34] drew the peripheral blood immune cell profile of patients with CRC, but their study only focused on T-, NK-, and NKT cell subsets. Additionally, these studies have laid a good foundation for exploring the changes of PBMC during the development of intestinal adenocarcinoma.

Currently, few studies have focused on depicting the immune microenvironment of adenoma. Adenoma is the key stage of adenocarcinoma carcinogenesis, and inhibiting adenoma has been proven to greatly reduce the occurrence of adenocarcinoma.[35,36] Using multi-region

Table 1. Major characteristic changes in circulating immune cell subpopulations during colorectal carcinogenesis

Cell type	Subpopulations markers	Subpopulations	Differently expression between groups
T cells	$CD56^+CD3^+CD45RA^+CD94^+CD57^+CD38^+$	Natural killer T cell	Adenoma > adenocarcinoma > normal
	$CD27^+CD45RA^+CCR7^+CD38^+CD127^+$	Double-negative T cell ($CD4^-CD8^-$)	Normal > adenoma > adenocarcinoma
	$CD25^+ICOS^+CD38^+CD39^+CCR4^+HLA^-DR^+CD4^+$	Regulatory T cell	Adenocarcinoma > adenoma
B cells	$CD85j^+CD39hiCD27^+CD45RA^+IgD^-CD38hi$	Switched Memory B cell	Adenocarcinoma > normal
	$CD19^+CD45RA^+CXCR5^+HLA^-DR^+$	Plasmablast	No metastatic > metastatic
NK cells	$CD56^+CD11c^+CD38^+HLA^-DR^+$	$CD16^-$ NK cell	Adenocarcinoma > adenoma > normal
Myeloid Cells	$CD14^+CD85j^+CD39^+CD86^+CD11c^{++}CD33^{++}$ $CD45^+CD38^+HLA^-DR^+CD11b^+$	Monocyte	Adenocarcinoma > adenoma > normal; stage I adenocarcinoma > adenoma
	$CD123^+HLA^-DR^-CD33^+CD45ROloCD38hiCD11b^+$	Basophil	Adenocarcinoma > adenoma; stage I adenocarcinoma > adenoma; no metastasis > metastasis

genome and exome sequencing of 24 benign and malignant colorectal tumors, Cross et al.[36] investigated the evolutionary fitness landscape occupied by these neoplasms. They found that advanced adenomas frequently harbor sub-clonal driver mutations considered to be functionally important in the carcinogenic process and have relatively high genetic heterogeneity. Studies have found[37] that eosinophils are recruited into developing tumors during induction of inflammation-induced CRC and in mice with the Apc min/+ genotype, which developed spontaneous intestinal adenomas.

The present study used CyTOF technology to perform PBMC detection of 102 CRC patients, 42 healthy people, and 47 adenoma patients. We clustered and selected the obtained cells based on the expression of 40 markers on the surface of PBMC cells, and a map of peripheral blood immune cells during the natural formation of intestinal adenocarcinoma was drawn. Compared with HC, the Treg cells in CRA increased, and the naive $CD8^+$ T in CRA and CRC decreased. Compared with CRA, naive $CD4^+$ T cells had higher expression in CRC, compared with HC and CRA. The naive B cells were significantly lower in CRC. Compared with stage II adenocarcinomas, the effector $CD4^+$ T cells were increased in stage III adenocarcinoma. In addition, we also found that compared with HC and CRA, the NKT cell was significantly reduced in CRC. NKT cells can not only activate various immune cells but also rejuvenate depleted immune cells in the tumor microenvironment and fight tumors by connecting innate and adaptive immunity. Some clinical trials based on NKT cell immunotherapy are already underway. Krijgsman et al.'s study[34] suggested that NK cell receptor ligands expressed by tumor cells may modulate the phenotype of circulating NK- and NKT cells and facilitate immune escape of metastasizing cells. Their another study[38] was consistent with our findings. Gharagozloo et al.[39] also found that there was a significantly lower number of $NKG2D^+$ $CD56^+$ NKT cells in the peripheral blood of patients with metastatic CRC compared with HC by flow cytometry.

Besides, we discovered that in the natural process of adenocarcinoma formation, the expression of a cell subset of Naive DNT ($CD27^+$ $CD45RA^+CCR7^+CD38^+CD127^{lo}$) was gradually decreasing. DNTs have been reported to have dual effects of killing tumor cells and inhibiting graft-versus-host disease. It was worth noting that DNTs can be obtained and amplified from healthy donors. Compared with HC, switched memory B cells were higher in CRC, and no other literature has reported the expression of switched memory B cells in CRC and the changes in each stage of cancer. Compared with non-metastatic CRC patients, plasmablasts were lower in metastatic CRC patients. Previous studies reported that in CRC, $CD19^+CD27^+$ plasma cells accounted for a large proportion of tumor-infiltrating lymphocytes and had strong immune regulation functions.

We discovered that in the process of adenoma occurrence and carcinogenesis, the peripheral blood content of a special type of $CD16^-$ NK cell ($CD56^+CD11c^+CD38^+HLA\text{-}DR^+$) was gradually increasing, whereas $CD16^+$ NK cells decreased in adenoma and adenocarcinoma. This is an extremely interesting finding. Compared with HC and CRA, $CD16^-$ monocyte cells were significantly higher in CRC. Compared with CRA, $CD16^+$ monocyte cell subsets were significantly reduced in CRC, and basophils cells were significantly increased in CRC patients. Haak et al.[40] investigated CRC infiltration by OX40 and CD16 expressing cells in 441 primary CRCs using tissue microarrays and specific antibodies, by immunohistochemistry. They found that combined infiltration by $OX40^+$ and $CD16^+$ immune cells is an independent favorable prognostic marker in CRC. The results of our study showed that compared with HC and CRA, the content of $CD16^+$ monocytes in stage I/II CRC was significantly higher, which suggested that $CD16^+$ monocytes may also be used as a marker for CRC. Previous studies on basophils in patients with CRC mainly focused on tumor proliferation and metastasis, and few studies reported the level of basophils in the adenoma stage. Although retrospective studies had also found basophils were elevated in CRC, the results of these studies were not consistent.[41,42] There was also no research on basal granulocyte subpopulations. Consequently, we conducted a detailed analysis and comparison of the basophil subpopulations in the peripheral blood of CRA and CRC. The content in stage II CRC was increased; compared with HC, the content of $CD123^+$ $CD11b^+$ basophils was increased in stage I CRC, which suggested that these subpopulations can also be used as marker cell subsets for early screening of CRC.

Limitations of the study

Although our study included large sample size, we did not perform CyTOF or single-cell sequencing detection on normal, adenoma, and adenocarcinoma tissues, which made our results based on peripheral blood PBMC studies not compared with the infiltration of immune cells in solid tissues for the time being. Considering that there was almost no single-cell level research on common adenomas (except FAP), we needed to further pay attention to the specific situation of immune cell infiltration in adenomas in subsequent research and identified and confirmed the corresponding cell subsets through basic experiments such as immunofluorescence.

Conclusions

The immune microenvironment of colorectal cancer (CRC) is not well studied in peripheral blood levels, and its alterations throughout the adenocarcinoma formation process are not well described in current research. In this work, we map peripheral blood immune cells at the single-cell level in the development of colorectal cancer. We created a sizable population cohort and investigated alterations in different immune cell subsets in the peripheral blood of colorectal cancer patients using CyTOF, employing the random forest algorithm to determine that monocytes are essential for the development of cancer. This study offers references for the immunoprofiling of other tumor types as well as prospective biomarkers for upcoming immunotherapy.

STAR★METHODS

Detailed methods are provided in the online version of this paper and include the following:

- KEY RESOURCES TABLE
- RESOURCE AVAILABILITY
  - Lead contact
  - Materials availability
  - Data and code availability
- EXPERIMENTAL MODEL AND STUDY PARTICIPANT DETAILS
  - Ethical approval and consent to participate
- METHOD DETAILS
  - Cytof measurement
  - Data process and analysis
  - Prediction of cancer-related cell subpopulations
  - Flow cytometry
- QUANTIFICATION AND STATISTICAL ANALYSIS
- ADDITIONAL RESOURCES

SUPPLEMENTAL INFORMATION

Supplemental information can be found online at https://doi.org/10.1016/j.isci.2024.109229.

ACKNOWLEDGMENTS

Thanks to Yong-Mao Song, Jian-Wei Wang, Li-Feng Sun, Hong-Feng Cao, Hua Ren, Xiu-Jun Liao, Qian Xiao, Da Wang, Jin-Jie He, Jing-Jing Zhang, Li-Mian Ling, Yang Tang, Yue Liu, Shao-Jun Yu, Qun Deng, and Feng Yu in our department for their contributions in sample collection. This research was supported by the National Natural Science Foundation of China (82103684, 11932017 to X.-X.K., 82172851 to J.L., 82072624 to K.-F.D.), Huadong Medicine Joint Funds of the Zhejiang Provincial Natural Science Foundation of China under Grant No. LHDMY22C060002 to X.-X.K., and the Fundamental Research Funds for the Central Universities (No.226-2022-00009) to K.-F.D.

AUTHOR CONTRIBUTIONS

X.-X.K. and J.-S.X. designed the experiment and wrote the manuscript. Y.-T.H. and Y.-R.J. collected the samples and revised the manuscript. S.C., C.-X.Y., and S.-Q.D. helped to revise the manuscript and language. Z.-B.G. and X.-R.H. conducted the CyTOF analysis. J.L. and K.-F.D. guided the study design and manuscript revision.

DECLARATION OF INTERESTS

The authors declare no competing interests.

Received: September 25, 2023
Revised: December 13, 2023
Accepted: February 8, 2024
Published: February 15, 2024

REFERENCES

1. Sung, H., Ferlay, J., Siegel, R.L., Laversanne, M., Soerjomataram, I., Jemal, A., and Bray, F. (2021). Global Cancer Statistics 2020: GLOBOCAN Estimates of Incidence and Mortality Worldwide for 36 Cancers in 185 Countries. CA. Cancer J. Clin. *71*, 209–249. https://doi.org/10.3322/caac.21660.
2. Fearon, E.R., and Vogelstein, B. (1990). A genetic model for colorectal tumorigenesis. Cell *61*, 759–767. https://doi.org/10.1016/0092-8674(90)90186-i.
3. Leslie, A., Carey, F.A., Pratt, N.R., and Steele, R.J.C. (2002). The colorectal adenoma-carcinoma sequence. Br. J. Surg. *89*, 845–860. https://doi.org/10.1046/j.1365-2168.2002.02120.x.
4. Bond, J.H. (1995). Interference with the adenoma-carcinoma sequence. Eur. J. Cancer *31a*, 1115–1117. https://doi.org/10.1016/0959-8049(95)00213-3.
5. (2012). Comprehensive molecular characterization of human colon and rectal cancer. Nature *487*, 330–337. https://doi.org/10.1038/nature11252.
6. Malla, M., Loree, J.M., Kasi, P.M., and Parikh, A.R. (2022). Using Circulating Tumor DNA in Colorectal Cancer: Current and Evolving Practices. J. Clin. Oncol. *40*, 2846–2857. https://doi.org/10.1200/jco.21.02615.
7. Pantel, K., and Alix-Panabières, C. (2019). Liquid biopsy and minimal residual disease - latest advances and implications for cure. Nat. Rev. Clin. Oncol. *16*, 409–424. https://doi.org/10.1038/s41571-019-0187-3.
8. Yu, J., Feng, Q., Wong, S.H., Zhang, D., Liang, Q.Y., Qin, Y., Tang, L., Zhao, H., Stenvang, J., Li, Y., et al. (2017). Metagenomic analysis of faecal microbiome as a tool towards targeted non-invasive biomarkers for colorectal cancer. Gut *66*, 70–78. https://doi.org/10.1136/gutjnl-2015-309800.
9. Kwong, T.N.Y., Wang, X., Nakatsu, G., Chow, T.C., Tipoe, T., Dai, R.Z.W., Tsoi, K.K.K., Wong, M.C.S., Tse, G., Chan, M.T.V., et al. (2018). Association Between Bacteremia From Specific Microbes and Subsequent Diagnosis of Colorectal Cancer. Gastroenterology *155*, 383–390.e8. https://doi.org/10.1053/j.gastro.2018.04.028.
10. Liu, W., Zhang, X., Xu, H., Li, S., Lau, H.C.H., Chen, Q., Zhang, B., Zhao, L., Chen, H., Sung, J.J.Y., and Yu, J. (2021). Microbial Community Heterogeneity Within Colorectal Neoplasia and its Correlation With Colorectal Carcinogenesis. Gastroenterology *160*, 2395–2408. https://doi.org/10.1053/j.gastro.2021.02.020.
11. Nakatsu, G., Li, X., Zhou, H., Sheng, J., Wong, S.H., Wu, W.K.K., Ng, S.C., Tsoi, H., Dong, Y., Zhang, N., et al. (2015). Gut mucosal microbiome across stages of colorectal carcinogenesis. Nat. Commun. *6*, 8727. https://doi.org/10.1038/ncomms9727.
12. Zheng, C., Zheng, L., Yoo, J.K., Guo, H., Zhang, Y., Guo, X., Kang, B., Hu, R., Huang, J.Y., Zhang, Q., et al. (2017). Landscape of Infiltrating T Cells in Liver Cancer Revealed by Single-Cell Sequencing. Cell *169*, 1342–1356.e16. https://doi.org/10.1016/j.cell.2017.05.035.
13. Guo, X., Zhang, Y., Zheng, L., Zheng, C., Song, J., Zhang, Q., Kang, B., Liu, Z., Jin, L., Xing, R., et al. (2018). Global characterization of T cells in non-small-cell lung cancer by single-cell sequencing. Nat. Med. *24*, 978–985. https://doi.org/10.1038/s41591-018-0045-3.
14. Gentles, A.J., Newman, A.M., Liu, C.L., Bratman, S.V., Feng, W., Kim, D., Nair, V.S., Xu, Y., Khuong, A., Hoang, C.D., et al. (2015). The prognostic landscape of genes and infiltrating immune cells across human cancers. Nat. Med. *21*, 938–945. https://doi.org/10.1038/nm.3909.
15. Galon, J., Costes, A., Sanchez-Cabo, F., Kirilovsky, A., Mlecnik, B., Lagorce-Pagès, C., Tosolini, M., Camus, M., Berger, A., Wind, P., et al. (2006). Type, density, and location of immune cells within human colorectal tumors predict clinical outcome. Science *313*, 1960–1964. https://doi.org/10.1126/science.1129139.
16. Pagès, F., Berger, A., Camus, M., Sanchez-Cabo, F., Costes, A., Molidor, R., Mlecnik, B., Kirilovsky, A., Nilsson, M., Damotte, D., et al. (2005). Effector memory T cells, early metastasis, and survival in colorectal cancer. N. Engl. J. Med. *353*, 2654–2666. https://doi.org/10.1056/NEJMoa051424.
17. Pagès, F., Kirilovsky, A., Mlecnik, B., Asslaber, M., Tosolini, M., Bindea, G., Lagorce, C., Wind, P., Marliot, F., Bruneval, P., et al. (2009). In situ cytotoxic and memory T cells predict outcome in patients with early-stage colorectal cancer. J. Clin. Oncol. *27*, 5944–5951. https://doi.org/10.1200/jco.2008.19.6147.
18. Pagès, F., Mlecnik, B., Marliot, F., Bindea, G., Ou, F.S., Bifulco, C., Lugli, A., Zlobec, I., Rau, T.T., Berger, M.D., et al. (2018). International validation of the consensus Immunoscore for the classification of colon cancer: a prognostic and accuracy study. Lancet *391*, 2128–2139. https://doi.org/10.1016/s0140-6736(18)30789-x.
19. Zhang, L., Yu, X., Zheng, L., Zhang, Y., Li, Y., Fang, Q., Gao, R., Kang, B., Zhang, Q., Huang, J.Y., et al. (2018). Lineage tracking reveals dynamic relationships of T cells in colorectal cancer. Nature *564*, 268–272. https://doi.org/10.1038/s41586-018-0694-x.
20. Zhang, L., Li, Z., Skrzypczynska, K.M., Fang, Q., Zhang, W., O'Brien, S.A., He, Y., Wang, L., Zhang, Q., Kim, A., et al. (2020). Single-Cell Analyses Inform Mechanisms of Myeloid-Targeted Therapies in Colon Cancer. Cell *181*, 442–459.e29. https://doi.org/10.1016/j.cell.2020.03.048.
21. Liu, Y., Zhang, Q., Xing, B., Luo, N., Gao, R., Yu, K., Hu, X., Bu, Z., Peng, J., Ren, X., and Zhang, Z. (2022). Immune phenotypic linkage between colorectal cancer and liver metastasis. Cancer Cell *40*, 424–437.e5. https://doi.org/10.1016/j.ccell.2022.02.013.
22. Bandura, D.R., Baranov, V.I., Ornatsky, O.I., Antonov, A., Kinach, R., Lou, X., Pavlov, S., Vorobiev, S., Dick, J.E., and Tanner, S.D. (2009). Mass cytometry: technique for real time single cell multitarget immunoassay based on inductively coupled plasma time-of-flight mass spectrometry. Anal. Chem. *81*, 6813–6822. https://doi.org/10.1021/ac901049w.
23. Finotello, F., Rieder, D., Hackl, H., and Trajanoski, Z. (2019). Next-generation computational tools for interrogating cancer immunity. Nat. Rev. Genet. *20*, 724–746. https://doi.org/10.1038/s41576-019-0166-7.
24. Gubin, M.M., Esaulova, E., Ward, J.P., Malkova, O.N., Runci, D., Wong, P., Noguchi, T., Arthur, C.D., Meng, W., Alspach, E., et al. (2018). High-Dimensional Analysis Delineates Myeloid and Lymphoid Compartment Remodeling during Successful Immune-Checkpoint Cancer Therapy. Cell *175*, 1014–1030.e19. https://doi.org/10.1016/j.cell.2018.09.030.
25. Steele, N.G., Carpenter, E.S., Kemp, S.B., Sirihorachai, V.R., The, S., Delrosario, L., Lazarus, J., Amir, E.A.D., Gunchick, V., Espinoza, C., et al. (2020). Multimodal Mapping of the Tumor and Peripheral Blood Immune Landscape in Human Pancreatic Cancer. Nat. Cancer *1*, 1097–1112. https://doi.org/10.1038/s43018-020-00121-4.
26. Zhang, Q., Ye, M., Lin, C., Hu, M., Wang, Y., Lou, Y., Kong, Q., Zhang, J., Li, J., Zhang, Y., et al. (2023). Mass cytometry-based peripheral blood analysis as a novel tool for early detection of solid tumours: a multicentre study. Gut *72*, 996–1006. https://doi.org/10.1136/gutjnl-2022-327496.
27. Dong, C., Ding, Y., Weng, S., Li, G., Huang, Y., Hu, H., Zhang, Z., Zhang, S., and Yuan, Y. (2021). Update in version 2021 of CSCO guidelines for colorectal cancer from version 2020. Chin. J. Cancer Res. *33*, 302–307.
28. Ge, P., Wei, W., Li, L., Zhang, G., Gao, Z., Tang, Z., Dang, X., and Wu, Y. (2019). Profiles of immune cell infiltration and immune-related genes in the tumor microenvironment of colorectal cancer. Biomed. Pharmacother. *118*, 109228.
29. Guo, L., Wang, C., Qiu, X., Pu, X., and Chang, P. (2020). Colorectal Cancer Immune Infiltrates: Significance in Patient Prognosis and Immunotherapeutic Efficacy. Front. Immunol. *11*, 1052.
30. Chen, J.H., Zhai, E.T., Yuan, Y.J., Wu, K.M., Xu, J.B., Peng, J.J., Chen, C.Q., He, Y.L., and Cai, S.R. (2017). Systemic immune-inflammation index for predicting prognosis of colorectal cancer. World J. Gastroenterol. *23*, 6261–6272. https://doi.org/10.3748/wjg.v23.i34.6261.
31. Matsutani, S., Shibutani, M., Maeda, K., Nagahara, H., Fukuoka, T., Iseki, Y., Hirakawa, K., and Ohira, M. (2018). Verification of the methodology for evaluating tumor-infiltrating lymphocytes in colorectal cancer. Oncotarget *9*, 15180–15197.
32. Li, M., Wang, H., Li, W., Peng, Y., Xu, F., Shang, J., Dong, S., Bu, L., Wang, H., Wei, W., et al. (2020). Identification and validation of an immune prognostic signature in colorectal cancer. Int. Immunopharmacol. *88*, 106868. https://doi.org/10.1016/j.intimp.2020.106868.
33. Zhang, T., Lv, J., Tan, Z., Wang, B., Warden, A.R., Li, Y., Jiang, H., Li, H., and Ding, X. (2019). Immunocyte Profiling Using Single-Cell Mass Cytometry Reveals EpCAM(+) CD4(+) T Cells Abnormal in Colon Cancer. Front. Immunol. *10*, 1571. https://doi.org/10.3389/fimmu.2019.01571.
34. Krijgsman, D., de Vries, N.L., Skovbo, A., Andersen, M.N., Swets, M., Bastiaannet, E., Vahrmeijer, A.L., van de Velde, C.J.H., Heemskerk, M.H.M., Hokland, M., and Kuppen, P.J.K. (2019). Characterization of circulating T-NK-and NKT cell subsets in patients with colorectal cancer: the peripheral blood immune cell profile. Cancer Immunol. Immunother. *68*, 1011–1024. https://doi.org/10.1007/s00262-019-02343-7.
35. Satoh, K., Yachida, S., Sugimoto, M., Oshima, M., Nakagawa, T., Akamoto, S., Tabata, S., Saitoh, K., Kato, K., Sato, S., et al. (2017). Global metabolic reprogramming of colorectal cancer occurs at adenoma stage and is induced by MYC. Proc. Natl. Acad. Sci.

USA *114*, E7697–E7706. https://doi.org/10.1073/pnas.1710366114.

36. Cross, W., Kovac, M., Mustonen, V., Temko, D., Davis, H., Baker, A.M., Biswas, S., Arnold, R., Chegwidden, L., Gatenbee, C., et al. (2018). The evolutionary landscape of colorectal tumorigenesis. Nat. Ecol. Evol. *2*, 1661–1672. https://doi.org/10.1038/s41559-018-0642-z.
37. Reichman, H., Itan, M., Rozenberg, P., Yarmolovski, T., Brazowski, E., Varol, C., Gluck, N., Shapira, S., Arber, N., Qimron, U., et al. (2019). Activated Eosinophils Exert Antitumorigenic Activities in Colorectal Cancer. Cancer Immunol. Res. *7*, 388–400. https://doi.org/10.1158/2326-6066.Cir-18-0494.
38. Krijgsman, D., Roelands, J., Andersen, M.N., Wieringa, C.H.L.A., Tollenaar, R.A.E.M., Hendrickx, W., Bedognetti, D., Hokland, M., and Kuppen, P.J.K. (2020). Expression of NK cell receptor ligands in primary colorectal cancer tissue in relation to the phenotype of circulating NK- and NKT cells, and clinical outcome. Mol. Immunol. *128*, 205–218. https://doi.org/10.1016/j.molimm.2020.10.012.
39. Gharagozloo, M., Rezaei, A., Kalantari, H., Bahador, A., Hassannejad, N., Maracy, M., Nouri, N., Sedghi, M., Ghazanfari, H., and Bayat, B. (2018). Decline in peripheral blood NKG2D+CD3+CD56+ NKT cells in metastatic colorectal cancer patients. Bratisl. Lek. Listy *119*, 6–11. https://doi.org/10.4149/bll_2018_002.
40. Haak, F., Obrecht, I., Tosti, N., Weixler, B., Mechera, R., Däster, S., von Strauss, M., Delko, T., Spagnoli, G.C., Terracciano, L., et al. (2020). Tumor Infiltration by OX40+ Cells Enhances the Prognostic Significance of CD16+ Cell Infiltration in Colorectal Cancer. Cancer Control *27*, 1073274820903383. https://doi.org/10.1177/1073274820903383.
41. Zhou, R., Zhang, J., Zeng, D., Sun, H., Rong, X., Shi, M., Bin, J., Liao, Y., and Liao, W. (2019). Immune cell infiltration as a biomarker for the diagnosis and prognosis of stage I-III colon cancer. Cancer Immunol. Immunother. *68*, 433–442. https://doi.org/10.1007/s00262-018-2289-7.
42. Zhang, X., Quan, F., Xu, J., Xiao, Y., Li, X., and Li, Y. (2020). Combination of multiple tumor-infiltrating immune cells predicts clinical outcome in colon cancer. Clin. Immunol. *215*, 108412. https://doi.org/10.1016/j.clim.2020.108412.
43. Finck, R., Simonds, E.F., Jager, A., Krishnaswamy, S., Sachs, K., Fantl, W., Pe'er, D., Nolan, G.P., and Bendall, S.C. (2013). Normalization of mass cytometry data with bead standards. Cytometry A *83*, 483–494. https://doi.org/10.1002/cyto.a.22271.
44. Zunder, E.R., Lujan, E., Goltsev, Y., Wernig, M., and Nolan, G.P. (2015). through progression analysis of single-cell mass cytometry. Cell Stem Cell *16*, 323–337. https://doi.org/10.1016/j.stem.2015.01.015.
45. van der Maaten, L., and Hinton, G. (2008). Visualizing data using t-sne. J. Mach. Learn. Res. *9*, 2579–2605.
46. Stassen, S.V., Siu, D.M.D., Lee, K.C.M., Ho, J.W.K., So, H.K.H., and Tsia, K.K. (2020). PARC: ultrafast and accurate clustering of phenotypic data of millions of single cells. Bioinformatics *36*, 2778–2786. https://doi.org/10.1093/bioinformatics/btaa042.
47. Samusik, N., Good, Z., Spitzer, M.H., Davis, K.L., and Nolan, G.P. (2016). Automated mapping of phenotype space with single-cell data. Nat. Methods *13*, 493–496. https://doi.org/10.1038/nmeth.3863.
48. Levine, J.H., Simonds, E.F., Bendall, S.C., Davis, K.L., Amir, el-AD, Tadmor, M.D., Litvin, O., Fienberg, H.G., Jager, A., Zunder, E.R., et al. (2015). Data-driven phenotypic dissection of AML reveals progenitor-like cells that correlate with prognosis. Cell *162*, 184–197. https://doi.org/10.1016/j.cell.2015.05.047.

STAR★METHODS

KEY RESOURCES TABLE

REAGENT or RESOURCE	SOURCE	IDENTIFIER
Antibodies		
CD45	Biolegend	Cat# 304002; RRID: AB_314390
CD3	Bioxcell	Cat# BE0231; RRID: AB_2687713
CD56	BD	Cat# 559043; RRID: AB_397180
TCR-g/d	PLT	100P001A Immunostep Cat# MJDF-05MG, RRID: AB_11140673
CD196/CCR6	Biolegend	Cat# 353402; RRID: AB_10918625
CD14	Biolegend	Cat# 301862; RRID: AB_2814125
IgD	Biolegend	Cat# 348202, RRID: AB_10550095
CD123/IL-3R	Biolegend	Cat# 306002; RRID: AB_314576
CD85j(ILT2)	Biolegend	Cat# 333722; RRID: AB_2814224
CD19	Biolegend	Cat# 302268; RRID: AB_2832580
CD25/IL-2R	RD	MAB1020 Diaclone Cat# 852.013.020; RRID: AB_596265
CD274/PD-L1	Biolegend	Cat# 329716; RRID: AB_11149168
CD278/ICOS	Biolegend	Cat# 313502; RRID: AB_416326
CD39	Biolegend	Cat# 328202; RRID: AB_940438
CD27	Biolegend	Cat# 302802; RRID: AB_314294
CD24	Biolegend	Cat# 311102; RRID: AB_314851
CD45RA	Biolegend	Cat# 304102; RRID: AB_314406
CD86	BD	Cat# 555655; RRID: AB_396010
CD28	Biolegend	Cat# 302934; RRID: AB_11148949
CD197/CCR7	Biolegend	Cat# 353256; RRID: AB_2814291
CD11c	Biolegend	Cat# 337202; RRID: AB_1236381
CD33	Biolegend	Cat# 303419; RRID: AB_2562818
CD152/CTLA-4	eB	Cat# 14-1529-82; RRID: AB_467512
CD161(NKR-P1A)	Biolegend	Cat# 339902; RRID: AB_1501090
CD185/CXCR5	BD	Cat# 552032; RRID: AB_394324
CD66b	Biolegend	Cat# 305102; RRID: AB_314494
CD183/CXCR3	Biolegend	Cat# 353750; RRID: AB_2810565
CD94	BD	Cat# 555887; RRID: AB_396199
CD57	Biolegend	Cat# 359602; RRID: AB_2562403
CD45RO	Biolegend	Cat# 304202; RRID: AB_314418
CD127/IL-7Ra	Biolegend	Cat# 351302; RRID: AB_10718513
CD279/PD-1	Biolegend	Cat# 329926; RRID: AB_11147365
CD38	Biolegend	Cat# 303502; RRID: AB_314354
CD194/CCR4	Biolegend	Cat# 359402; RRID: AB_2562364
CD20	Biolegend	Cat# 302302; RRID: AB_314250
CD16	Biolegend	Cat# 302057; RRID: AB_2572005
HLA-DR	Biolegend	Cat# 307648; RRID: AB_2561493
CD4	Bioxcell	Cat# BE0288; RRID: AB_2687811
CD8a	Biolegend	Cat# 301074; RRID: AB_2814117

(*Continued on next page*)

Continued

REAGENT or RESOURCE	SOURCE	IDENTIFIER
CD11b	Biolegend	Cat# 101202; RRID: AB_312785
Biological samples		
whole blood	This paper	N/A
Chemicals, peptides, and recombinant proteins		
1640 basal culture medium	Shanghai Basalmedia Technologies Co., Ltd.	L220KJ
Cell isolates	GE HealthCare	17-0891-09
Lymphocyte separation medium	GE HealthCare	17-1440-03
Red Cell Lysis Solution	zhejiang Puluoting Health Tech Co., Ltd.	BS-01-05
DNA enzyme	Sigma-Aldrich	D5025-150KU
Collagenase	Sigma-Aldrich	V900893
phorbol ester	Intech Bio-chem. Co. Limited	00-4975-93
phytohemagglutin phytolectin	gibco(Thermo Fisher Scientific)	10576–015
The Golgi apparatus blockers	Intech Bio-chem. Co. Limited	00-4980-93
Monomycin	Aladdin Biochemical Technology Co., Ltd	M118287
bovine serum albumin	Sigma-Aldrich	V900933
benzo blue	Beijing Solarbio Science & Technology Co., Ltd.	C0040
194 Cisplatin dead live stain	Fluidigm Corporation, USA	201194
DNA stain	Fluidigm Corporation, USA	201192B
Alignment Particle	Fluidigm Corporation, USA	201078
cleaning solution	Fluidigm Corporation, USA	201070
DAPI Staining reagent	ServiceBio Co., LTD	G1012
Anti-fluorescence-quenching-sealing tablets	ServiceBio Co., LTD	G1401
RNA ScreenTape Sample Buffer	Agilent	5067–5577
OptiPrepDensity gradient culture medium	Sigma	D1556
Protector RNase inhibitor	Roche	3335402001
bovine serum albumin	sigma	A1933-25G
Fetal bovine serum(FBS)	RAININ	A3161001C
Nuclease-Free Water (not DEPC-Treated)	Invitrogen	AM9937
1X TE buffer solution	Thermo	12090015
PCR Tubes,0.2 mL,PCR	Eppendorf	30124332
SPRIselect Reagent	BECKMAN	B23318
Critical commercial assays		
Antibody metal labeling kit	Fluidigm Corporation, USA	201300
RNeasy FFPE Mini kit(50)	Qiagen	73504
RNase-Free DNase Set (50)	Qiagen	79254
Library Quantification Kits	KAPA	7960000000
Single Index Kit T Set A	10x Genomics	1000213
Chromium Next GEM Chip G Single Cell Kit	10x Genomics	1000120
Chromium Next GEM Single Cell Library Kit v3.1	10x Genomics	1000121
Chromium Next GEM Single Cell 3′GEM Gel Bead Kit v3.1	10x Genomics	1000122
Software and algorithms		
FlowJo v10.0.7	BD	https://www.flowjo.com/
Normalizer	Finck et al.[43]	https://github.com/nolanlab/bead-normalization

(*Continued on next page*)

Continued

REAGENT or RESOURCE	SOURCE	IDENTIFIER
Single cell debarcoder	Zunder et al.[44]	https://github.com/nolanlab/single-cell-debarcoder
t-SNE	van der Maaten and Hinton[45]	https://github.com/jkrijthe/Rtsne
PARC	Stassen et al.[46]	https://github.com/ShobiStassen/PARC
X-shift	Samusik et al.[47]	https://github.com/nolanlab/vortex
PhenoGraph	Levine et al.[48]	https://github.com/jacoblevine/PhenoGraph

RESOURCE AVAILABILITY

Lead contact

Further information and requests for resources and reagents should be directed to and will be fulfilled by the lead contact, Prof. Ke-Feng Ding (dingkefeng@zju.edu.cn).

Materials availability

This study did not generate new unique reagents.

Data and code availability

Relevant test data in the study have been uploaded to the OMIX database (website: https://ngdc.cncb.ac.cn/omix/submitList), Number: OMIX005724. All data reported in this paper will be shared by the lead contact upon request. This paper does not report original code. Any additional information required to reanalyze the data reported in this paper is available from the lead contact upon request.

EXPERIMENTAL MODEL AND STUDY PARTICIPANT DETAILS

All patients were prospectively enrolled during August 2020 and October 2020 from the second affiliated hospital of Zhejiang University, school of Medicine. The inclusion and exclusion criteria were listed in Table S1. Patients were classified into three groups based on colonoscopy and pathological reports. HC, is defined as healthy controls, whose colonoscopy confirmed with no occupying lesions. CRA, is defined as patients only diagnosed with pathology confirmed adenoma. CRC, is defined as patients diagnosed with pathology confirmed adenocarcinoma, without any non-adenocarcinoma malignant tumors or distant metastasis. Patient characteristics for samples used in the study are listed in Table S2.

This study was approved by the ethics committee of the Second Affiliated Hospital, Zhejiang University School of Medicine (2021-LYS-0473). Consents were signed by all participants. Clinical information was collected from the hospital information system. Five microliters of peripheral blood were collected before colonoscopy for routine tests and CyTOF analysis.

Ethical approval and consent to participate

This study was conducted in accordance with the recommendations of the Ethics Committee of the Second Affiliated Hospital of Zhejiang University(2021-LYS-0473). The protocol was adopted by the Ethics Committee of the Second Affiliated Hospital of Zhejiang University. All subjects gave written informed consent in accordance with the Declaration of Helsinki.

METHOD DETAILS

Cytof measurement

EDTA-treated whole blood was lysed using ACK lysis buffer to obtain PBMCs by Ficoll density gradient centrifugation. Cold cell staining buffer was used to resuspend the pellet. Cells were collected by centrifugation at 300g for 5 min at 2°C–8°C. We then labeled single-cell suspension using 194Pt for 5 min to distinguish live from dead. Forty immune cell markers (details in Table S3) were used to stain PBMCs. The stained PBMCs were sorted using the Porting CyTOF platform. At least 300,000 single cells were extracted from PBMCs from each patient. CyTOF analysis was performed by PLTTech Inc. (Hangzhou, China).

Data process and analysis

Data generated from different batches were normalized and then de-barcoded using a doublet filtering scheme with mass-tagged barcodes and manually gated to retain live, singlet, valid immune cells. All cell events in each sample have been pooled and used for clustering. We used CyTOF software v6.7 to merge and standardize collected data. Cytobank (https://www.cytobank.org/) and several R packages (cytofkit, Rtsne, FlowSOM, cytofexplorer, ggplots et al.) were used to analyze data. We used the t-distributed stochastic neighborhood embedding (t-SNE) algorithm through viSNE to perform t-SNE dimensionality reduction analysis and generate t-SNE visualization results. Leukocytes in PBMCs were screened by CD45. We performed heatmap analysis of the expression of 40 markers in all samples, followed by cluster analysis

of all $CD45^+$ cells. Cell types of each subgroup were determined by prior knowledge and cell marker database annotation. PhenoGraph was used to cluster cell subgroups and comparatively analyze their characteristics.

Prediction of cancer-related cell subpopulations

We screened differential markers between the HC and CRA. We applied the random forest algorithm to filter the differential markers. The mean decrease in Gini coefficient (Mean Decrease Gini, MDG) was calculated using the importance function to rank cell markers. We scored the markers' difference to remove the gradient effect and constructed neural network models via the Neural Net Tools package to clarify how these markers matched each other to characterize CRC.

Flow cytometry

PBMCs were collected from 20 participants from G1, G2,and G3, respectively. Cells were stained with CD14 and CD16 double indicators, and we also conducted a blank control group without stain. The fluorescence intensity of the four groups of samples was analyzed by flow cytometry and compared between groups.

QUANTIFICATION AND STATISTICAL ANALYSIS

Statistical analysis was conducted using R projects (version 4.3.0). Data was expressed as mean ± standard deviation (SD) or as medians with interquartile ranges. Statistical significance between the two groups was calculated using non-parametric Mann-Whitney test. Rejection of the null hypothesis with a p value < 0.05 was considered significant.One asterisk (*) indicates a p value <0.05, two asterisks (* *) indicates a p value <0.01, and three asterisks (* * *) indicates a p value <0.001.

ADDITIONAL RESOURCES

This study involves data and materials collected from patients enrolled in Clinical Trial: ClinicalTrials.gov ID: NCT04074538.